Liquid-State Theory of Semidilute and Concentrated Polymer Solutions

Avik P. Chatterjee and Kenneth S. Schweizer*

Departments of Materials Science & Engineering and Chemistry, and Materials Research Laboratory, University of Illinois, 1304 West Green Street, Urbana, Illinois 61801

Received October 6, 1997; Revised Manuscript Received January 15, 1998

ABSTRACT: We present a theory for thermodynamic and equation-of-state properties of polymer solutions over the entire concentration range, and for homopolymer melts, based on analytic polymer reference interaction site model (PRISM) methods. A single polymer is modeled as either an effectively Gaussian thread, or as a Gaussian string which approximately accounts for the effects of a nonzero chain thickness. Both good (athermal) and Θ solvent conditions are considered within a molecular closure approximation scheme. Good agreement is found with experimentally measured second and third virial coefficients, and with the osmotic pressure and screening length, in dilute and semidilute athermal solutions. Experimentally observed deviations from the power law dependence on chain length (N) of the athermal second and third virial coefficients is interpreted in terms of finite segmental hard core interchain packing effects at low molecular weights; these finite size effects are predicted to vanish in the limit $N \rightarrow \infty$. For long chains in the semidilute regime the theory predicts the irrelevance of the finite size of the segments, in accord with scaling and field theoretic approaches. The breakdown of power law scaling behavior for the screening length and osmotic pressure is identified with the emergence of the concentrated solution regime at roughly 25−30% volume fraction of polymer. For concentrated solutions and melts, calculations of the equation of state based on the string model show good agreement with simulations of athermal chains for appropriately chosen model parameters. Comparison with experimental PVT data for polyethylene melts at elevated temperatures and pressures shows that the analytic theory provides an accurate description of the temperature and pressure dependences of the isothermal compressibility and the coefficient of thermal expansion.

I. Introduction

The theory of polymer solutions is of abiding interest owing to sources of complexity and phenomena which have no counterparts in mixtures of simple (atomic) fluids. Despite a long history of research in this area,[1−4] unanswered questions and challenges remain. It is the aim of this work to take the first step toward developing a unified analytic theoretical treatment of polymer solutions based on liquid-state integral equation methods, which is applicable to solutions spanning the entire experimental range of concentrations.

It is customary to classify polymer solutions into three concentration regimes: dilute, semidilute, and concentrated.[1,2] The dilute regime corresponds to concentrations low enough that, to a good approximation, one may treat individual chains as independent, non-interacting coils, which under good solvent conditions behave almost as hard spheres with a size given by the radius of gyration R_g. Solution thermodynamics in this regime can be described by the virial coefficients, which may be evaluated from cluster expansion methods.[3] Fujita[5] has recently summarized a number of outstanding unresolved issues in dilute polymer solutions. For example, questions remain regarding an experimentally observed upturn in the N dependence of the second virial coefficient B_2 at low molecular weights for solutions of polystyrene (PS) in toluene. The intermediate semidilute concentration regime represents a situation unique to polymer solutions, in which individual coils overlap and interpenetrate even though the concentration of polymer on a volume fraction basis can be quite minute.[1−4] The structure and thermodynamics of solutions in this regime have been explored using scaling[2] and field theoretical ideas,[6,7] and renormalization group methods,[8] which successfully describe the experimentally observed power law concentration dependence of the osmotic pressure[1] and the density screening length[9] or mesh size. However, these methods cannot generally predict at which (higher) concentration they cease to be applicable, that is, the onset of the concentrated or meltlike regime. The concentrated regime is characterized by a density screening length which is comparable to or smaller than nonuniversal length scales such as the chain persistence length or monomer dimension, and by an osmotic pressure that rises increasingly rapidly in a non-power-law fashion as a function of polymer volume fraction.[10] In this regime, statistical thermodynamic mean field approaches such as the generalized Flory dimer (GFD) model[10−12] provide a good description of the steeply increasing pressure; however, such models give an inaccurate description of the N-dependence of the virial coefficients relevant to the dilute regime, and fail to capture the power-law scaling behavior in semidilute solutions due to strong monomer correlation effects. No theoretical framework that correctly captures the characteristic thermodynamic features in all three concentration regimes, predicts the boundaries between them, and describes the smooth crossover effects has been developed on the basis of traditional methods of polymer physics.

In the present work, we propose a theory for polymer solutions over the entire range of concentrations, using methods of liquid-state theory developed initially for fluids of small molecules[13] and later extended to treat macromolecular systems.[14] For simplicity, the present model treats the solution as an effective one-component system, in which the concentration is varied by altering the density of the polymeric component; the solvent degrees of freedom are not treated explicitly. In addition, this initial study does not determine the single-

S0024-9297(97)01460-5 CCC: $15.00
Published on Web 03/12/1998

chain structure self-consistently; rather, where necessary, an effective concentration-dependent statistical segment length is employed with a Gaussian chain description in the spirit of field theoretical approaches.[6,7] In contrast to the latter approaches based on crossable thread chains, the local hard core excluded volume constraint is accounted for in an approximate manner. We find that this minimalistic analytically tractable model, which does not include the effects of local chain stiffness or monomer shape, provides a satisfactory description of many aspects of the solution thermodynamics in all three concentration regimes. The theory also provides the foundation within the polymer reference interaction site model (PRISM) framework for analytically treating the influence of a constant pressure constraint, and attendant "equation-of-state" effects, on polymer blend phase behavior, including the lower critical solution temperature (LCST) phenomenon.[15] Our primary focus is on good solvent (athermal) conditions, though a few calculations under thermal and Θ point conditions are also presented. The latter aspect provides the foundation for treating thermally induced phase transitions, such as the homopolymer liquid−vapor transition, as discussed elsewhere.[16]

The remainder of this article is organized as follows. In section II, we define the model and provide a brief summary of our theoretical methods. In section III, the theory for athermal/purely repulsive systems is developed. Section IV treats thermal effects on the virial coefficients and calculation of the Θ temperature and attractive contributions to the equation of state. In section V, we present the predictions of our theory and comparisons to experimental data in the dilute, semidilute, and melt-like regimes. All the results discussed in the body of this article make use of the compressibility route to the thermodynamics; a discussion of predictions from the free energy route is given in the Appendix.

II. PRISM Theory

Within the polymer reference interaction site model (PRISM), the site-averaged Ornstein−Zernike equation for a one-component homopolymer fluid takes the form[14]

$$\hat{h}(k) = \hat{\omega}(k)\,\hat{C}(k)[\hat{\omega}(k) + \rho_m \hat{h}(k)] \equiv \hat{\omega}(k)\,\hat{C}(k)\,\hat{S}(k) \quad (1)$$

where $\hat{h}(k)$ and $\hat{C}(k)$ represent the Fourier-transformed site−site intermolecular total and direct correlation functions, respectively, $g(r) \equiv 1 + h(r)$ is the corresponding intermolecular radial distribution function, ρ_m is the site number density, and $\hat{\omega}(k)$ is the single-chain structure factor normalized such that $\hat{\omega}(k=0) = N$, where N is the number of interaction sites per polymer chain. For chains with finite hard core diameter d, eq 1 is supplemented by the exact hard core constraint:

$$g(r) = 0, \quad r < d \quad (2)$$

Most work to date for finite diameter hard core chains has employed the accurate site−site Percus−Yevick approximation for treating the reference athermal system:[13,14]

$$C^{(0)}(r) = 0, \quad r > d \quad (3)$$

where $C^{(0)}(r)$ represents the reference-state (athermal) site−site direct correlation function. Alterations in the polymer concentration in solution are modeled by varying the site number density ρ_m. We follow the standard method used in liquid-state theory of separating the intersite pair potential into "reference" (hard core)/athermal and "perturbative"/attractive ($v(r)$) branches.[17] Given our treatment in terms of an effective one-component system, the potential between segments would be expected to contain three- and higher-body terms arising from the integration over solvent degrees of freedom, *even if the underlying microscopic interactions are rigorously pairwise additive.*[3] In the present work we ignore this complication and *assume* that the intersite potentials in the effective one-component system are pairwise additive. The treatment of attractive interactions within a molecular closure framework is discussed in section IV.

In principle, the single-chain structure and intermolecular correlations must be determined self-consistently. A variety of methodologies within the PRISM framework have been developed recently to accomplish this,[18−22] although their implementation is somewhat complex. Our present initial study avoids the full self-consistent treatment and adopts a simpler analytic approximation for $\hat{\omega}(k)$, appropriate for effectively Gaussian chains in a continuum-like limit:[1]

$$\hat{\omega}(k) = \frac{1}{1/N + k^2\sigma^2/12} \quad (4)$$

where σ is an effective statistical segment length which may be density/concentration-dependent to account for changes in chain dimensions under good solvent conditions. Adoption of this model allows analytic results to be derived on the basis of PRISM theory, and connections to blob scaling and field theoretical approaches to be most clearly elucidated.

The compressibility route to the thermodynamics is adopted. The isothermal compressibility κ_T follows from the zero-wavevector value of the direct correlation function, $C(0)$, or the static structure factor, $S(k=0) \equiv S_0$, as[14]

$$\rho_m k_B T \kappa_T = S_0 = \frac{N}{1 - \rho_m N C(0)} \quad (5)$$

The compressibility route (osmotic) pressure is then obtained by a density charging or integration process:

$$\beta P = \int_0^{\rho_m} d\rho_1\, S_0^{-1}(\rho_1) \quad (6)$$

The motivation for employing the compressibility route includes its technical ease of implementation, the emphasis on $k = 0$ correlations which seems most appropriate for a theory based on a coarse-grained Gaussian chain model, and the theoretical difficulties inherent to the free energy charging route (see Appendix and refs 16 and 23).

III. Analytic Results for Athermal Solutions

Athermal solutions, defined by $v(r) \equiv 0$, represent the limiting good solvent condition where polymer segments interact solely via pairwise hard core potentials.

A. Thread Model. Many prior analytic PRISM studies have made use of the $d \to 0$ Gaussian thread idealization,[14] for which the purely athermal direct correlation function in eq 1 within the PY closure is approximated by a δ-function at the origin in position space with an amplitude parameter C_0:

$$C(r) = C_0\delta(\mathbf{r}) \tag{7}$$

The hard core constraint in eq 2 is replaced by the requirement that $g^{(0)}(r)$ for the reference athermal thread system vanishes as $r \to 0$. For the $\omega(k)$ in eq 4, the reference thread pair correlation function is given by[14]

$$g^{(0)}(r) = 1 + \frac{3}{\pi\rho_m\sigma^2 r}[e^{-r/\xi_\rho} - e^{-r/\xi_c}] \tag{8}$$

where the correlation hole length scale ξ_c is related to the coil radius of gyration R_g by

$$\xi_c^{\,2} = \frac{N\sigma^2}{12} = R_g^{\,2}/2 \tag{9}$$

and the density screening length ξ_ρ satisfies

$$\frac{\sigma}{\xi_\rho} = \frac{\sigma}{\xi_c} + \frac{\pi\rho_m\sigma^3}{3} \tag{10}$$

The reference-state direct correlation strength parameter, C_0, is given by

$$12C_0\rho_m = \sigma^2[\xi_c^{\,-2} - \xi_\rho^{\,-2}] \tag{11}$$

The reciprocal of the density-dependent collective structure factor at $k = 0$ is thus

$$S_0^{\,-1}(\rho_m) = \frac{1}{12}\left[\frac{\pi\rho_m\sigma^3}{3} + \frac{\sigma}{\xi_c}\right]^2 \tag{12}$$

From eqs 6 and 12, the pressure for the athermal thread fluid is

$$\beta\sigma^3 P = \frac{z}{N} + \frac{\pi z^2}{36}\left(\frac{\sigma}{\xi_c}\right) + \frac{\pi^2 z^3}{324}, \quad z \equiv \rho_m\sigma^3 \tag{13}$$

From eq 13, the second and third virial coefficients B_2 and B_3 for the athermal thread model are given by

$$B_2(N) = \frac{\pi\sigma^3}{3\sqrt{12N}} \propto \frac{R_g^{\,3}}{N^2}, \quad B_3 = \frac{\pi^2\sigma^6}{324} \tag{14}$$

The virial series terminates with B_3 for the athermal thread model. Note that the second virial coefficient B_2 in eq 14 is proportional to the volume of a single coil; this corresponds to the classic idea[2,3] that in dilute solution the chains behave as non-interacting hard spheres of radius R_g. In a dilute good solvent, chains are swollen compared to their ideal dimensions; that is, $R_g \sim N^{\nu_F}$ where ν_F equals 0.5 under ideal conditions but is greater for a good solvent. Renormalization group calculations yield the estimate[1] $\nu_F = 0.588...$, and experiments[24−26] on polystyrene (PS) in toluene find $\nu_F \approx 0.59-0.6$; for the qualitative discussion of this section, we shall use the Flory mean field value[1−3] of $\nu_F = 0.6$. In analogy with field theoretical approaches,[1,4,6,7] the departure of ν_F from 0.5 can be accommodated in our simple Gaussian model by requiring the segment length σ to obey

$$\sigma \sim N^{(\nu_F - 1/2)} \sim N^{0.1} \tag{15}$$

The $N-$dependences of B_2 and B_3 in a good solvent are then predicted to be

$$B_2 \sim N^{(3\nu_F - 2)} \sim N^{-0.2}, \quad B_3 \sim N^{(6\nu_F - 3)} \sim N^{0.6} \tag{16}$$

The above predictions are consistent with the observed experimental behavior[24−26] of PS in toluene at high molecular weights. Equation 14 shows that, for the athermal thread model, the ratio B_3/NB_2^2 equals $^1/_3$, *independent* of the Flory exponent ν_F. This prediction compares favorably with the results of MC simulations on a variety of lattices, which find that $B_3/NB_2^2 \approx 0.3$ in the long-chain limit,[27] and with the conclusion of a renormalization group theoretical estimate[28] that this ratio approaches an asymptotic value of 0.277.

For a solution of chains with coil radius R_g, we identify the density ρ_m^* for the crossover between dilute and semidilute solution regimes from the standard coil overlap condition:[1−3]

$$\rho_m^* = \frac{N}{\frac{4}{3}\pi R_g^{\,3}} \tag{17}$$

which leads to the relation that $\rho_m^* \sim N^{(1-3\nu_F)}$. For the case of a semidilute solution of polymer in a good solvent, scaling theory and experiments suggest that the radius of gyration, which is proportional to ξ_c, depends on the density of polymer in the system. The prediction of scaling theory,[1,2] or self-consistent PRISM theory for athermal thread polymer solutions,[20] that

$$R_g^{\,2} \sim \rho_m^{\,-(1-2\nu_F)/(1-3\nu_F)} \tag{18}$$

is incorporated in our model by requiring the effective segment length to obey

$$\sigma \sim \rho_m^{\,-(1-2\nu_F)/2(1-3\nu_F)} \tag{19}$$

in the semidilute regime. Use of eq 19 in the expression for ξ_ρ in eq 10 in the limit that $N \to \infty$ yields the semidilute regime PRISM prediction:

$$\xi_\rho \sim \rho_m^{\,\nu_F/(1-3\nu_F)} \tag{20}$$

which is again consistent with scaling theory[1,2] and experiment.[9] If we use the mean-field value $\nu_F = 0.6$, eqs 13 and 19 predict in the semidilute regime

$$\beta P(\rho_m) \sim \rho_m^{\,9/4} \tag{21}$$

in agreement with scaling theory[1,2] and experimental osmotic pressure measurements.[29] It is noteworthy that within field theoretical approaches the results of eqs 20 and 21 follow only if repulsive three-body interactions are included, in contrast to PRISM theory, where only two-body bare potentials are employed but a renormalized effective potential, C_0, enters in order to enforce the interchain hard core impenetrability constraint.

In the hypothetical limit that $\rho \to \infty$, eq 13 predicts that the repulsive contribution to the pressure increases as $P \sim z^3$, a much slower rate of increase than found in computer simulations or equation-of-state theories of athermal chains at meltlike packing fractions.[10−12] This shortcoming is a consequence of the neglect of the finite range ($d \neq 0$) of interchain excluded volume interactions at the thread polymer level of treatment. For understanding the properties of concentrated solutions (where

$d \geq \xi_\rho$), it is important to account for the fact that $g(r) = 0$ for $0 < r < d$, as opposed to the condition used in eq 8. This consideration motivates study of the so-called Gaussian string model.[14]

B. String Model. In the analytically tractable "string model",[30] the reference-state direct correlation function is again approximated as a spatial δ-function, but the hard core exclusion constraint is enforced over a region of diameter d around each monomer in the following average way:

$$\int_0^d \mathrm{d}r\, g_0(r) r^2 = 0 \tag{22}$$

The theoretical basis for eq 22 as an optimized perturbative treatment of finite hard core models in terms of an effectively threadlike reference fluid has been previously established.[14,30] The athermal pair correlation function for the string model is identical in form to eq 8 for the thread model, but the density correlation length ξ_ρ satisfies the following transcendental equation:[14,30,31]

$$\frac{\xi_c}{d}\left(\frac{\xi_c}{d}+1\right)\mathrm{e}^{-d/\xi_c} - \left(\frac{\xi_\rho}{d}\right)\left(\frac{\xi_\rho}{d}+1\right)\mathrm{e}^{-d/\xi_\rho} + \left(\frac{\xi_\rho^{\,2}}{d^2} - \frac{\xi_c^{\,2}}{d^2}\right) = -\frac{\pi\rho_m\sigma^3}{9\Gamma} \tag{23}$$

$$\Gamma = \sigma/d \tag{24}$$

where Γ can be loosely interpreted as a chain aspect ratio. In the limit that the hard core diameter vanishes ($d \to 0$), one can show that eq 23 leads to the expression given in eq 10 for the thread model. Further simplification of eq 23 follows in the limit that $\xi_c/d \to \infty$, which can be achieved by taking $N \to \infty$ at fixed d:

$$x^2(1 - \mathrm{e}^{-1/x}) - x\mathrm{e}^{-1/x} = \frac{1}{2} - \frac{\pi\rho_m\sigma^3}{9\Gamma}, \quad x = \xi_\rho/d \tag{25}$$

Equation 25 can be shown to have a unique solution for ξ_ρ/d as a function of density for $0 < z \equiv \rho_m\sigma^3 < 9\Gamma/2\pi$; for values of z exceeding $9\Gamma/2\pi$, there are no real and positive solutions to the above equation. Imposition of the excluded volume constraint, albeit in an average way, leads to the existence of an upper limit to the monomer density ρ_m, above which physical solutions to the PRISM equation do not exist. Such a singularity is presumably a consequence of the oversimplified string model approximation that $\hat{C}(k) \equiv \hat{C}(0) \equiv C_0$. However, within the string model, it could be interpreted as corresponding to the total site packing fraction associated with an incompressible close-packed fluid state. Introducing a new rescaled density variable ψ, defined as

$$\psi = z/\Gamma = \rho_m\sigma^3/\Gamma \tag{26}$$

the dependence of ξ_ρ on model parameters can be written as

$$(\xi_\rho/\sigma) = \frac{f(\psi)}{\Gamma} \tag{27}$$

where $f(\psi)$ is a function of ψ alone, defined implicitly by comparison with eq 25. As ψ approaches the upper limit at which solutions to eq 25 cease to exist, it is found that ξ_ρ becomes vanishingly small:

$$(\xi_\rho/\sigma) \sim \frac{1}{\sqrt{2\Gamma}}\sqrt{1 - \psi/\psi_{max}}, \quad \psi_{max} \equiv \frac{9}{2\pi} \tag{28}$$

The above behavior has important consequences on the compressibility route pressure calculated for the reference state:

$$P^* \equiv d^3\beta P_{rep}(\psi) = \frac{1}{12}\int_0^\psi d\psi_1 \frac{1}{f^2(\psi_1)} = F(\psi) \tag{29}$$

Equation 28 implies that P^* diverges logarithmically in the vicinity of ψ_{max}:

$$d^3\beta P_{rep}(\psi) \sim \ln\left(\frac{1}{\psi_{max} - \psi}\right) \tag{30}$$

Logarithmic divergence of the athermal pressure is found also in the Sanchez−Lacombe lattice treatment of the homopolymer fluid;[32,33] in that case, the pressure divergence occurs when the lattice occupancy (η) approaches unity. Power-law divergence of the athermal pressure at a continuous space packing fraction of $\eta = 1$ is predicted by the approximate PY theory of the hard sphere fluid,[17] and occurs also in the exact solution of the one-dimensional fluid of hard rods.[34] Inspection of eqs 26 and 28 reveals that, as the segment length σ increases keeping d fixed, the site density at which the athermal pressure diverges *decreases* ($\rho_{max} \sim 1/\sigma^2 d$). If one interprets the process of increasing the aspect ratio Γ at fixed d as analogous to enhancing the local chain stiffness, the concomitant decrease in $\rho_m{}^{max}$ is consistent with the general physical picture that stiffer chains "pack better", resulting in a larger number of interchain contacts, a reduced compressibility, and hence an enhanced athermal pressure, relative to those of more flexible chains.[14]

We note that the dependence of ξ_ρ and P^* on ψ and Γ implied in eqs 28 and 30 holds only in the limit in which $\Gamma\xi_\rho \to 0$. In the semidilute regime, eq 25 yields

$$(\xi_\rho/\sigma) \approx \frac{3}{\pi\rho_m\sigma^3}; \quad \rho_m \to 0, \quad N \to \infty, \quad \rho_m/\rho_m{}^* \gg 1 \tag{31}$$

consistent with the prediction of the thread model in this limit. Remarkably, for long chains at such relatively low semidilute polymer concentrations, the dependence of ξ_ρ on Γ, and thereby on the segment diameter d, *drops out completely*. Thus, the microscopic PRISM theory predicts the "irrelevance" of local chemical length scales such as d and Γ for the polymer concentration dependence of the screening length, osmotic pressure, and other semidilute solution properties in accord with phenomenological scaling ideas.[2]

For finite chain lengths N, one can obtain from eq 23 expressions for the athermal solution virial coefficients as expansions in powers of (d/R_g); the first-order corrections to the second and third virial coefficients are given by

$$B_2(N) = \frac{\pi\sigma^3}{36\xi_c}\left[1 + \frac{3}{4R} + ...\right], \quad B_3(N) = \frac{\pi^2\sigma^6}{324}\left[1 + \frac{9}{4R} + ...\right] \tag{32}$$

where

$$R = \xi_c/d = R_g/\sqrt{2}d \tag{33}$$

The leading-order contributions to both B_2 and B_3 in eq 32 are precisely given by the PRISM results for the thread model. As expected, the corrections due to the finite segment diameter d become more important as N decreases. For both B_2 and B_3, the correction corresponds to an *increase* in the virial coefficients; that is, the repulsive pressure is enhanced relative to the thread model prediction. Additionally, the string model differs from the thread in that the pressure virial series no longer terminates with B_3 but contains nonzero contributions from all orders in ρ_m.

We have so far focused on calculating the osmotic pressure within the compressibility route. A discussion of the athermal pressure for the string model calculated using the free energy charging route is included in the Appendix. It is there shown that, as expected for *any* liquid-state theory, the two routes to the thermodynamics are quantitatively inconsistent with each other and yield different expressions for B_3. However, the ρ_m scaling laws for βP and ξ_ρ in the semidilute regime are identical for the two routes. But, we also find that B_3 obtained using the charging route does *not* in general lose its dependence on Γ *or* reduce to the thread result on taking the limit $d \to 0$, except in the very special case that $\Gamma^4 = 13.5$. Thus the free energy charging route predictions would seem to violate a basic tenet of universality and scaling. We note that the compressibility route calculation relies on the accuracy of the calculated zero-wavevector structure factor S_0, whereas the free energy route requires a precise calculation of $g^{(0)}(r)$ *locally*. The latter may be expected to be more inaccurately described by coarse-grained Gaussian thread or string models and our approximate treatment of the local hard core constraint.

Additional deficiencies of the charging route predictions follow from examination of the contact value of $g(r)$, that is, $g_c = g(r=d)$. In the athermal string fluid it may be found from eq 8 to be

$$g_c = 1 + \frac{3}{\pi\psi}[e^{-d/\xi_\rho} - 1] \tag{34}$$

As the quantity ξ_ρ/d is a function only of ψ in the long chain limit, it follows that g_c is also a function of ψ alone and is otherwise independent of Γ. Clearly, g_c is bounded above by $^1/_3$, and since the pressure calculated in the virial route is related to the contact value of $g(r)$, the free energy route pressure calculated in the Appendix does *not* diverge as $\psi \to \psi_{max}$. At low densities, and in the limit $N \to \infty$, a virial expansion can be developed for ξ_ρ/d in powers of ψ from eq 25:

$$\frac{d}{\xi_\rho} = \frac{\pi\psi}{3} + \frac{\pi^2\psi^2}{24} + O(\psi^3) \tag{35}$$

Use of eq 35 in eq 34 for g_c yields the following expressions at low densities:

$$g_c \approx \pi\psi/24, \quad \xi_\rho g_c/d \to \frac{1}{8} \quad \text{as} \quad \psi \to 0 \tag{36}$$

The pressure calculated from the compressibility route is found to be in much better agreement with the results of simulations than that obtained from the free energy charging route. The basis for this conclusion is presented in the main part of Figure 1, where the athermal/reference system reduced pressure ($P/\rho_m k_B T$) as a function of packing fraction η for the string model is compared to the MD simulation data[10] obtained by Gao and Weiner for off-lattice, hard core tangent bead chains. It should be noted that mapping our model variables onto the variables relevant to the simulation is a two-step process. We need to establish a correspondence between our model density and the packing fraction in the simulation, and also must identify a specific value for the aspect ratio Γ. For the former question, the maximum density ψ_{max} in the string model is identified with the real system packing fraction of $\eta \approx 1/\sqrt{2}$, roughly the appropriate value for close-packed hard spheres; thus, for our model, the repulsive pressure diverges logarithmically as $\eta \to 1/\sqrt{2}$. The value of the aspect ratio Γ was then chosen to provide the best fit to the simulation data. We find that choosing $\Gamma \sim 10$ provides a reasonable fit to the data; in the figure shown, we have used $\Gamma = 10.3$. Using smaller values for Γ in this calculation leads to a pressure lower in magnitude than, and also less rapidly increasing in comparison to the simulation data. A value of $\Gamma \approx 10$ is difficult to justify a priori. However, we feel the agreement shown in Figure 1 is nevertheless rather impressive for a model which accounts so crudely for the excluded volume interaction and local chain structure and packing. Our assumption of a Gaussian form for the intrachain structure factor $\hat{\omega}(k)$, and the consequent neglect of local stiffness effects, is likely to be most questionable at high, melt-like densities. Shown also in Figure 1 is the prediction of the generalized Flory dimer (GFD) model[11,12] (dot−dash line), which ignores chain connectivity effects; with the fitting procedure described above, the string PRISM and GFD models describe the simulation data with comparable accuracy. The short- and long-dashed lines in Figure 1 show the much poorer predictions of the string model based on the free energy charging route and of the athermal thread model, respectively.

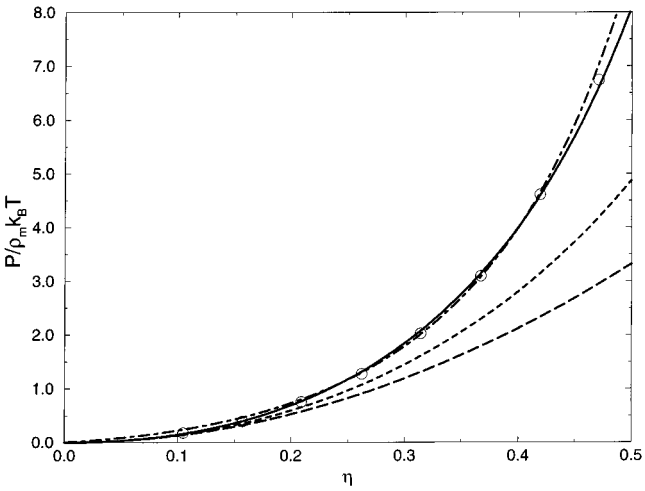

Figure 1. Reduced athermal pressure $P/\rho_m k_B T$ plotted as a function of packing fraction $\eta \equiv \pi\rho_m d^3/6$; the circles and solid line show the MD data[10] from simulations by Gao and Weiner for chains with $N = 200$ and from the string model prediction from the compressibility route, respectively. The short-dashed, long-dashed, and dot-dashed lines correspond to predictions of the athermal string model from the free energy charging route, the athermal thread model, and the athermal GFD equation of state,[11,12] respectively. The string model calculations shown in this figure use the aspect ratio $\Gamma = 10.3$.

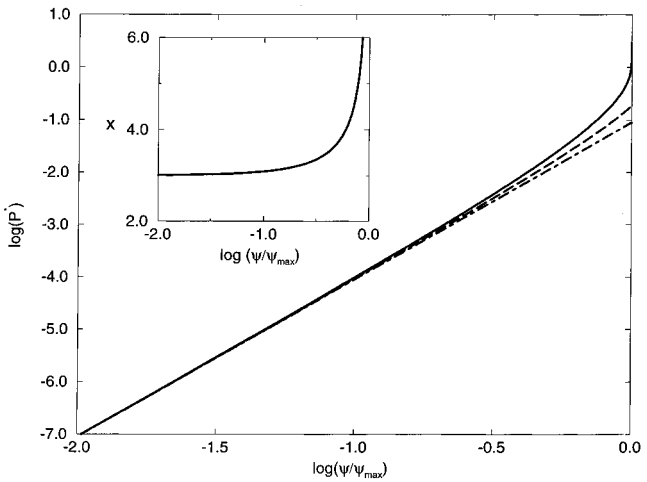

Figure 2. Logarithm of the reduced athermal pressure ($P^* \equiv Pd^3/k_BT$) plotted as a function of $\log(\psi/\psi_{max})$. The solid and dashed curves show the predictions of the athermal string model from the compressibility and free energy charging routes, respectively. The dot-dashed line represents the athermal thread model. The free energy charging route calculation displayed uses an aspect ratio Γ satisfying $\Gamma^4 = 13.5$. The inset shows the density-dependent effective exponent x defined as the derivative of $\log P^*$ with respect to $\log(\psi)$, as a function of $\log(\psi/\psi_{max})$, for the athermal string model from the compressibility route.

In Figure 2, the solid line shows the dimensionless pressure P^*d^3/k_BT for the athermal string fluid in the limit $N \rightarrow \infty$, calculated from eq 29 as a function of the reduced density ψ/ψ_{max} (eqs 26, 28, and 29). The dot−dash line shows the prediction of the athermal thread model, $P^* = \pi^2\psi^3/324$, and the dashed line shows the pressure calculated from the charging route as described in the Appendix; for this calculation we have used $\Gamma^4 = 13.5$, to enforce consistency with the compressibility route and the thread model results in the limit $\psi/\psi_{max} \rightarrow 0$. The inset shows the logarithmic density derivative of the compressibility route pressure, which defines the apparent density-dependent exponent on the basis of a forced power-law fit of the form $P^* \approx \psi^x$. Note that, for low and moderate ("semidilute") densities, there exists a regime in which $P^* \sim (\psi/\psi_{max})^3$. However, at higher densities, a stable ψ-independent effective exponent cannot be identified. The compressibility route pressure grows significantly faster than the thread prediction for $\psi/\psi_{max} > 0.15-0.2$, culminating in a logarithmic divergence as $\psi \rightarrow \psi_{max}$. At $\psi/\psi_{max} = 1/\sqrt{2}$, corresponding to a melt-like packing fraction $\eta = {}^1/_2$, we find that $P^* \sim (\psi/\psi_{max})^{4.5}$, that is, $x \approx 4.5$, for the athermal string model from the compressibility route. Since typical melt densities are expected to be $\eta \approx {}^1/_2$, we estimate that the semidilute-concentrated crossover density, ρ_m^{**}, corresponds to roughly 25−30% polymer volume fraction solutions, consistent with the limited experimental information for when the semidilute scaling laws break down.[9] Given the estimate that ρ_m^{**} corresponds to about 25−30% polymer volume fraction, and identification of the melt-like regime with $\psi/\psi_{max} \approx 1/\sqrt{2}$, solution of eq 25 shows that $\xi_\rho \approx 3 \pm 0.3d$ at ρ_m^{**} within the athermal string model, a reasonable value when compared with experimental measurements.[9]

IV. Thermal Effects and Θ Solutions

We now examine the influence of including an attractive intersite interaction. For phase-separating polymer blends, and also for block copolymer systems, the effects of attractive tail potentials on the liquid structure and thermodynamics have been successfully treated within PRISM theory using novel "molecular closures" formulated and discussed extensively in earlier work.[35−39] Our present analytic treatment employs the Reference Molecular Percus−Yevick/high-temperature approximation (RMPY/HTA) closure, which, for finite diameter chains, is defined by eq 1 together with[35,36]

$$\omega^*C^*\omega(r) = \omega^*C^{(0)}*\omega(r) + \omega^*\Delta C^*\omega(r), \quad r > d$$

$$\Delta C(r) = -\beta v(r)\, g^{(0)}(r), \quad r > d \tag{37}$$

where the asterisks denote r-space convolutions. Equations 1 and 37 are supplemented by the exact hard core condition (eq (2)). Mathematically, the RMPY/HTA represents a perturbative approximation in βv *at the level of the effective potential or the direct correlation function*. Physically, this closure approximation incorporates the influence of local packing in the reference fluid on the effect of the bare tail potential in a manner akin to the calculation of the fluid enthalpy or cohesive energy.

For the $d \rightarrow 0$ thread model, the convolutions in eq 37 may be canceled,[35,36] leading to the following expression for the Fourier transform of the site−site direct correlation function within the RMPY/HTA closure:

$$\hat{C}(k) = C_0 - \beta \int d\mathbf{r}\; v(r)\, g_0(r) e^{i\mathbf{k}\cdot\mathbf{r}} \tag{38}$$

We choose the attractive potential to be of truncated Yukawa form:

$$v(r) = 0, \quad r < d \tag{39}$$

$$v(r) = -|\epsilon|\left(\frac{a}{r}\right)e^{-r/a}, \quad r > d \tag{40}$$

The choice of a single Yukawa form to represent the attractive interaction is purely for analytic convenience. One may extend the present analysis to a potential representable by a sum over several Yukawa terms with different strength and range parameters, which could be chosen to mimic the presence of multiple wells or barriers. One could also choose the strength parameter in eq 40 to be positive, that is, to represent a repulsion of the screened-Coulombic form appropriate for polyelectrolyte solutions;[22] in this case, our system will exhibit neither a positive Θ temperature (see below) nor a liquid−gas transition. Within the context of the present effective one-component model for polymer solutions, $v(r)$ in eq 40 actually corresponds to an effective potential between polymer segments obtained after integrating out the solvent degrees of freedom. In general, such an effective potential would include thermal and packing-driven solvent-induced effects, which (phenomenologically) could make the strength and range parameters ϵ and a in eq 40 dependent on temperature and polymer concentration. A priori calculation of the solvent-induced aspects of $v(r)$ is not possible within the framework of a one-component model. For the purposes of the present work, which focuses mostly on athermal conditions, we disregard such complications and assume the potential parameters ϵ and a as defined by eq 40 to be intrinsic, that is, independent of the thermodynamic state of the system.

As documented elsewhere for the thread model,[16] the RMPY/HTA molecular closure within the compress-

ibility route provides a successful description of the liquid−vapor critical properties. In addition, the RMPY/HTA closure has been successfully employed to address numerous issues in polymer melts[40] (e.g., solubility parameters), blends,[37] and diblock copolymer thermodynamics and thermal phase behavior.[38,39] Most notably, for semidilute blend and diblock copolymer solutions, the thread PRISM with the RMPY/HTA closure has been shown to predict an effective χ parameter in good and Θ solvents which is consistent with renormalization group and blob scaling analyses.[41,42] It has also provided a microscopic explanation of the failure of the mean field "dilution approximation" for χ in concentrated copolymer solutions and melts.[42] Thus, we employ the RMPY/HTA closure exclusively in all the thermal work in this paper. The crucial physical aspect is the dependence of the attractive force direct correlation function (second term in eq 37) on reference system mesh size, that is, for large N:

$$\beta\int \mathrm{d}\mathbf{r}\; g_0(r)\; v(r)\mathrm{e}^{\mathrm{i}\mathbf{k}\cdot\mathbf{r}} = \frac{\beta\epsilon 4\pi a^3}{1+\xi_\rho/a} \tag{41}$$

For the thread model ($d \to 0$), the compressibility route using the RMPY/HTA closure (eq 37) yields for the osmotic pressure

$$\beta\sigma^3 P = \frac{\rho_\mathrm{m}\sigma^3}{N} + \left(\frac{\pi\rho_\mathrm{m}{}^2\sigma^6}{36}\right)\left(\frac{\sigma}{\xi_\mathrm{c}}\right) + \frac{\pi^2\rho_\mathrm{m}{}^3\sigma^9}{324} - \frac{2\pi}{T^*}\left(\frac{a}{\sigma}\right)^3\rho_\mathrm{m}{}^2\sigma^6 + \frac{12\rho_\mathrm{m}\sigma^3}{T^*(1+a/\xi_\mathrm{c})}\left(\frac{a}{\sigma}\right)^2 - \frac{36}{\pi T^*}\left(\frac{a}{\sigma}\right)\ln\left[1+\frac{\pi a\rho_\mathrm{m}\sigma^3}{3\sigma(1+a/\xi_\mathrm{c})}\right] \tag{42}$$

where

$$T^* = k_\mathrm{B}T/|\epsilon| \tag{43}$$

The presence of a thermal contribution that grows as $\sim \ln(\rho_\mathrm{m}\sigma^3)$ at large densities implies that the virial series no longer terminates with B_3; however, the cubic increase of P with density for $\rho_\mathrm{m} \gg \rho_\mathrm{m}{}^*$ is not affected. Expansion of the logarithm in eq 42 leads to expressions for the second and third virial coefficients modified by the attractive interactions:

$$B_2 = \pi\sigma^3\left(\frac{\sigma}{\xi_\mathrm{c}}\right)\left[\frac{1}{36} - \frac{2}{T^*}\left(\frac{a}{\sigma}\right)^4\left\{\frac{2+\frac{a}{\xi_\mathrm{c}}}{\left(1+\frac{a}{\xi_\mathrm{c}}\right)^2}\right\}\right]$$

$$B_3 = \pi^2\sigma^6\left[\frac{1}{324} - \frac{4(a/\sigma)^4}{9T^*(1+a/\xi_\mathrm{c})^3}\right] \tag{44}$$

Attractions reduce both virial coefficients relative to their athermal, purely repulsive values. We note that thermal corrections to the athermal values of the virial coefficients are *always* linear in $1/T^*$; this mathematical structure is a direct result of our use of the RMPY/HTA closure. The N-dependent Θ temperature, $T_\theta{}^*(N)$, defined as the value of T^* at which the second virial coefficient vanishes, is given by

$$T_\theta^*(N) = 144\left(\frac{a}{\sigma}\right)^4\frac{(1+a/2\xi_\mathrm{c})}{(1+a/\xi_\mathrm{c})^2} \tag{45}$$

In the limit that $N \to \infty$, the Θ temperature increases toward an N-independent limiting value, which we denote as Θ, given by

$$\Theta = 144\left(\frac{a}{\sigma}\right)^4 \tag{46}$$

For the $d \neq 0$ string model, use of the RMPY/HTA closure within the compressibility route leads to the following expression for the pressure:

$$\beta P(\rho_\mathrm{m}) = \frac{1}{12}\int_0^{\rho_\mathrm{m}} d\rho_1\left(\frac{\sigma(\rho_1)}{\xi_\rho(\rho_1)}\right)^2 - 2\pi a^3 A(1+1/\nu)\rho_\mathrm{m}{}^2 - 12Aa^2\int_0^{\rho_\mathrm{m}} d\rho_1\left(\frac{1}{\sigma^2(\rho_1)}\right)\left[\frac{\mathrm{e}^{-d/\xi_\rho(\rho_1)}}{(1+a/\xi_\rho(\rho_1))} - \frac{\mathrm{e}^{-d/\xi_\mathrm{c}(\rho_1)}}{(1+a/\xi_\mathrm{c}(\rho_1))}\right] \tag{47}$$

$$A = \frac{\mathrm{e}^{-1/\nu}}{T^*} \tag{48}$$

$$\nu = a/d \tag{49}$$

Note that in eq 47 we have allowed the segment length σ to be a function of polymer density or concentration. This feature is necessary for predicting the osmotic pressure in the semidilute good solvent regime.

The remainder of this section focuses on calculating the virial coefficients. From eq 23, a virial expansion for ξ_ρ/d, valid at small densities ψ and large values of ξ_c/d, can be derived:

$$\frac{d}{\xi_\rho} = \frac{1}{R} + \frac{\pi}{3}\left(1+\frac{3}{4R}\right)\psi + \frac{\pi^2\psi^2}{24} + \frac{29\pi^3\psi^3}{4320} + \ldots, \qquad R = \xi_\mathrm{c}/d \tag{50}$$

Substitution of eq 50 in eq 47 leads to the following expansions for the virial coefficients in powers of d/R_g:

$$B_2(N,T^*) = \pi\sigma^3\left(\frac{\sigma}{\xi_\mathrm{c}}\right)\left[\frac{1}{36}\left(1+\frac{3}{4R}+\ldots\right) + \frac{2A}{\Gamma^2}\left(\frac{\nu}{\Gamma}\right)^2\left\{\frac{-(8\nu^2+5\nu+1)}{4} + \frac{240\nu^3+21\nu+1}{80R} + \ldots\right\}\right] \tag{51}$$

$$B_3(N,T^*) = \frac{\pi^2\sigma^6}{18}\left[\left(\frac{1}{18}+\frac{1}{8R}+\ldots\right) - \frac{A}{\Gamma^2}\left(\frac{\nu}{\Gamma}\right)^2(8\nu^2+5\nu+1+O(1/R))\right] \tag{52}$$

$$B_4(N,T^*) = \frac{\pi^3\sigma^9}{\Gamma}\left[\frac{1}{1728} + \frac{A}{\Gamma^2}\left(\frac{\nu}{\Gamma}\right)^2\left\{\frac{29(1+\nu)}{1440} - \frac{(\nu^2+\nu+{}^1/_2)}{12} + \frac{(\nu^3+\nu^2+\nu/2+{}^1/_6)}{9} + O(1/R)\right\}\right] \tag{53}$$

For large N, the limiting Θ temperature is given by

$$\Theta = \frac{18(8\nu^2+5\nu+1)}{\Gamma_\theta{}^2}\left(\frac{\nu}{\Gamma_\theta}\right)^2\mathrm{e}^{-1/\nu} \tag{54}$$

Here, Γ_θ is the aspect ratio $\Gamma = \sigma/d$ at the Θ temperature. An expression for the second virial coefficent B_2 which contains terms to all orders in $1/R$, where $R \equiv R_g/\sqrt{2}d$, is obtained by evaluating the second density derivative of the pressure in eq 47. The result is

$$B_2 = -\left(\frac{\sigma^3}{12}\right)\left(\frac{\sigma}{\xi_c}\right)^3 \frac{\partial(\xi_\rho/\sigma)}{\partial z} - \frac{\pi\sigma^3}{9}\left(\frac{\Theta}{T^*}\right)\frac{{\Gamma_\theta}^4}{\Gamma^3}\frac{(1+\nu)}{(8\nu^2+5\nu+1)} - \frac{\sigma^3}{3}\left(\frac{\Theta}{T^*}\right)\frac{{\Gamma_\theta}^4}{\Gamma^2}\frac{e^{-d/\xi_c}}{\left(1+\frac{\nu d}{\xi_c}\right)^2(8\nu^2+5\nu+1)}\left[\frac{(1+\nu)\sigma d}{{\xi_c}^2} + \frac{\nu\sigma d^2}{{\xi_c}^3}\right]\frac{\partial(\xi_\rho/\sigma)}{\partial z} \quad (55)$$

$$\frac{\partial(\xi_\rho/\sigma)}{\partial z} = \frac{(\pi\xi_c/\sigma)}{9\Gamma[(2{\xi_c}^2/d^2 + 2\xi_c/d + 1)e^{-d/\xi_c} - 2{\xi_c}^2/d^2]} \quad (56)$$

where the derivatives with respect to density are evaluated at $z = 0$. A similar calculation yields an unwieldy expression for B_3 including terms of all orders in d/R_g which we shall use later but refrain from displaying explicitly.

V. Comparison with Experiments

In this section, we apply the theoretical results of sections III and IV to experimental measurements in dilute and semidilute good solutions and for concentrated solutions/melts.

A. Dilute Solution Virial Coefficients. From eq 51, one finds that, under athermal conditions, B_2 as calculated in the string model is larger than that predicted in the thread limit, but that the difference becomes progressively smaller as N is increased. Recall that, for the thread model with an N-independent Flory exponent ν_F, B_2 is predicted to exhibit a simple power law scaling, $B_2 \sim N^{(3\nu_F-2)}$ (eq 16). Thus, a double-logarithmic plot of the athermal B_2 predicted by the string PRISM model versus N is a decreasing function which is concave upward; in contrast, the $d \to 0$ thread model yields a straight line. This behavior is qualitatively consistent with measurements of B_2 for polystyrene (PS) in toluene[5]. Similar considerations hold for the third virial coefficient B_3; here again, within the assumption that ν_F is independent of N, the thread model predicts a simple power-law type behavior (eq 16), while the hard core constraint as implemented in the string model increases B_3, the effect being larger for shorter chains. Thus, for good solvents, eq 52 predicts that a double-logarithmic plot of B_3 versus N should also be concave upward, except that B_3 is a monotonically increasing function of N as opposed to B_2. The trends predicted above for B_2 and B_3 are now quantitatively compared with experimental measurements.

One of the more widely studied polymer plus good solvent systems is polystyrene (PS) in toluene. At the temperatures normally accessible to experiments ($T \approx$ 300−400 K), this system is effectively athermal[43] ($\Theta << 300$ K). Figure 3 compares the theoretical second virial coefficient B_2 with experimentally measured values (circles) for the PS plus toluene system[24−26,43−46] at temperatures between 283 and 308 K. The solid lines

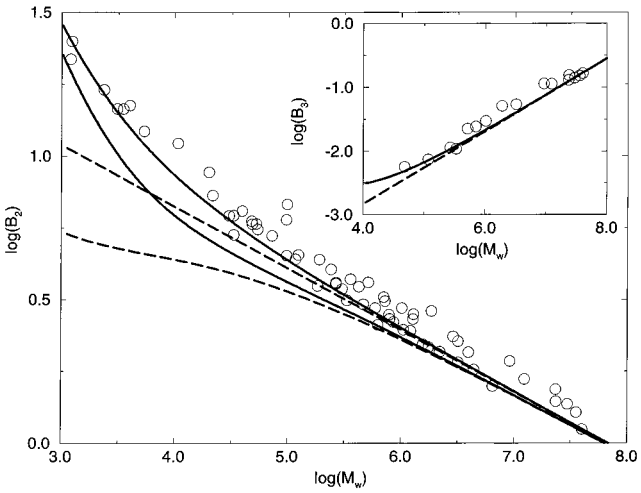

Figure 3. Logarithm of the second virial coefficient ($\log(B_2)$) in units of 10^{-4} cm^3 mol/g^2 plotted versus $\log(M_w)$ for PS in toluene. The circles show experimental data;[24−26,43−46] the solid and broken lines correspond to the predictions of the string and thread models, respectively. For each pair of lines, the upper member represents an athermal calculation, and the lower one corresponds to the temperature $T^* = 2\Theta$. The theoretical calculations employ an aspect ratio $\Gamma_\theta = 1$, $\sigma_\theta =$ 7.058 Å, and an effective Flory exponent of $\nu_F = 0.595$. The range of the potential a for the thermal calculations is $a = d/2$. The inset shows $\log(B_3)$ in units of cm^6 mol/g^2 as a function of $\log(M_w)$ for PS in toluene; the circles show experimental data,[24,25] and the solid and broken lines correspond to the athermal string and thread model predictions, respectively. The parameters used for the curves in the inset are the same as those in the main panel; details of the fitting procedure are described in the text.

are the prediction of the string model (eqs 55 and 56); the upper line is for an athermal system, and the lower one is at $T^* = 2\Theta$. In calculating B_2 for the string model, we have equated the number of monomers in the string model chain to the degree of polymerization in PS. The experimentally determined chain expansion factor for PS in toluene at high molecular weights[26] leads to the following equation for the ratio $\sigma(N)/\sigma_\theta$:

$$\frac{\sigma(N)}{\sigma_\theta} = 0.67\ N^{0.095} \quad (57)$$

Comparison of the large N values for the athermal B_2 calculated from eqs 55 and 56 with experimental data[25] allows us to determine $\sigma_\theta = 7.058$ Å, which corresponds to $C_\infty \approx 10.5$, in remarkably good agreement with the literature value[47] of $C_\infty = 10$ for PS in its Θ solvent cyclohexane. We use this value for σ_θ and eq 57 for the chain expansion factor in all the theoretically calculated curves in Figure 3. An aspect ratio of unity ($\Gamma_\theta = 1$) is employed, consistent with an a priori estimate which identifies $\pi d^3/6$ with the volume per monomer in PS melts.[40] The curves in Figure 3 thus represent a one-parameter fit to the experimental data. The athermal string model correctly predicts the observed concave-upward shape of the data to within experimental error. The physical origin of this feature is our inclusion of the $d \neq 0$ interchain excluded volume interaction; it is absent from the simpler thread model and scaling type arguments. The dashed lines in Figure 3 show the corresponding pure power-law predictions of the thread model (eq 44). As expected, lowering the temperature results in a reduction in B_2.

The inset in Figure 3 compares the athermal third virial coefficient B_3 calculated from the string and

thread models to experimental data for the PS plus toluene system.[24,25] The thread model prediction (eq 44) is represented by the broken line. Use of eq 57 to describe the N-dependence of R_g for all values of N implies that B_3 in the thread limit obeys a power law with no finite-size corrections. For the string model, the analogue of eqs 55 and 56 obtained for B_2 is utilized, and the present calculation includes terms to all orders in d/R_g. For the N dependence of the chain expansion factor and the numerical value of σ_θ, we employ the same values used in our previous comparison of B_2. The theoretical curves in the inset to Figure 3 thus represent a *zero-fit-parameter* prediction. As discussed in section III, the thread and string model predictions agree in the large-N regime, but, as N is decreased, B_3 calculated using the string model is greater than that predicted in the thread limit, leading to the concave-upward shape. The numerical agreement with the experimental measurements is satisfactory, especially for the set of measurements at the longest chain lengths.

Our comparisons to measurements of B_2 and B_3 in Figure 3 have employed the experimentally determined asymptotic expression for the N dependence of R_g over the entire range of molecular weights considered. Experimentally, it is found that the effective Flory exponent ν_F is slightly weaker[26] than its asymptotic value of 0.595 for $M < 10^5$. At ultralow molecular weights ($10^3 < M < 10^4$), there appears some ambiguity in the experimental findings; one group reports[26] an increase in ν_F, interpreted as due to chain stiffness effects, and other workers[48] find that ν_F remains at near its ideal value (0.5) down to $M = 5000$. In our theory, a decrease in the effective Flory exponent would *also* lead to an upturn and upward-concave shape for *both* B_2 *and* B_3; we see from eqs 51 and 52 that, if $\nu_F = 0.5$, then in the athermal limit we would expect $B_2 \sim N^{-1/2}$ and $B_3 \sim N^0$. The observed upturn in the N dependence of B_2 has been attributed to chain stiffness[26,49] or chain end[44] effects at low molecular weights. In our work, we have not been concerned with the details of the chain stiffness, intrachain excluded volume effects at low M, or chain end effects; instead, we demonstrate that an upturn in B_2 may be caused solely by the $d \neq 0$ interchain excluded volume interaction, even assuming that the chains obey simple self-avoiding-walk-like statistics at all molecular weights. It is necessary to reemphasize that the results shown in Figure 3 have assumed Gaussian chain statistics for *all* molecular weights, an assumption which is not really accurate for $N \leq 10^2$; the close numerical agreement between the experimentally measured and theoretically calculated virial coefficients for low-molecular-weight samples could thus be partly fortuitous.

As pointed out by the reviewer, experimental measurements of the molecular weight dependences of B_2 and B_3 for PS dissolved in benzene exhibit similar upturns and deviations from power-law behavior at low molecular weights.[50] The deviations in this case set in at larger molecular weights than those for PS in toluene; deviations from power-law dependence are apparent for $M_w \leq 10^6$ for B_2 and for $M_w \leq 10^5$ for B_3 for PS dissolved in benzene. A comparison with the athermal string model predictions has been carried out, making use of the experimentally determined M_w dependence of R_g. The procedure employed was identical to that adopted for PS dissolved in toluene, as discussed in connection with Figure 3, and involved *no* adjustable fitting parameters. Experimental determinations of the coil radius of gyration for PS in benzene[50] are consistent with the behavior $R_g \sim M_w^{0.605}$ over the range $2 \times 10^5 < M_w < 2 \times 10^7$. We refrain from presenting detailed results for this case but note that the level of quantitative agreement between theoretical and measured values of B_2 and B_3 is poorer than that for the case of PS in toluene. In particular, experiments find a more significant departure from power-law dependence at higher molecular weights than predicted by the theory, suggesting that factors other than finite chain thickness may also be involved in this phenomenon.

The foregoing comparisons have been made for the good solvent case. The situation is more complex for Θ solvents, where the Flory exponent $\nu_F = 0.5$. From eq 45, the thread model predicts that as N increases, T_θ^* approaches its limiting value Θ from below. At $T^* = \Theta$, the second virial coefficient in the thread model is

$$B_2(\Theta,N) = \frac{\pi\sigma_\theta^3}{3N}\left(\frac{a}{\sigma_\theta}\right)\left[\frac{\frac{3}{2} + \left(\frac{a}{\sigma_\theta}\right)\left(\frac{\sigma}{\xi_c}\right)}{\left(1 + \left(\frac{a}{\sigma_\theta}\right)\left(\frac{\sigma}{\xi_c}\right)\right)^2}\right] \qquad (58)$$

indicating that $B_2(T^* = \Theta,N)$ is positive definite for all values of N, and vanishes like $B_2 \sim 1/N$ in the large-N limit. That similar conclusions hold for the string model can be verified from eqs 51 and 54.

Experiments on PS in two different Θ solvents, cyclohexane (CH) ($\Theta = 307.65$ K) and *trans*-decalin ($\Theta = 294.15$ K), yield somewhat different results. For PS in CH,[44,49] it is found that B_2 is indeed positive at Θ for all N and becomes negligibly small for $M_w > 5 \times 10^4$; however, for PS in *trans*-decalin at $T = \Theta$, it is found that[51] B_2 is a nonmonotonic function of N. For large N, in *trans*-decalin, B_2 first decreases from zero to a negative value as M_w is reduced and then shows a sharp positive upturn[51] as M_w decreases below about 5×10^3. The observed monotonic increase in B_2 with decreasing N for PS in CH at Θ has been attributed to chain end effects which become important at low molecular weights.[44,52] This observation is qualitatively consistent with the prediction of eq 58 above; however, PRISM theory as employed here does *not* include explicit chain end effects. We see from eqs 45, 51, and 54 that the nonmonotonicity of $B_2(\Theta)$ as a function of N observed for PS in *trans*-decalin is not captured by either the thread or string models; this nonmonotonicity is thought to arise from residual ternary cluster integral contributions at the Θ point.[51] For the third virial coefficient, we find that the thread model at $T^* = \Theta$ predicts

$$B_3(\Theta,N) = \frac{\pi\sigma_\theta^6}{324}\left[1 - \frac{1}{\left(1 + \left(\frac{a}{\sigma_\theta}\right)\left(\frac{\sigma}{\xi_c}\right)\right)^3}\right] \qquad (59)$$

a positive definite expression vanishing in the large-N limit as $B_3 \sim 1/\sqrt{N}$. This prediction that B_3 vanishes at Θ in the long chain limit is contrary to experiments on PS in both CH[53] and *trans*-decalin,[51] which find that, at Θ, B_3 approaches a finite positive value independent of M. Examination of eqs 52 and 54 shows that the string model suffers from the same drawback. The presence of a contribution to B_3 at Θ which does not vanish in the long chain limit has been attributed to

contributions from the ternary cluster integral[51−53] (three-body interactions).

We conclude that our present models based on bare two-body interactions and nonperturbative liquid-state theory provide a satisfactory overall picture of the virial coefficients in the case of athermal or good solvents. However, important problems remain in the vicinity of $T = \Theta$, perhaps related to our neglect of *explicit* three-body interactions. Our microscopic treatment should be contrasted with field-theoretical approaches,[1−4,6,7] which use as a starting point phenomenologically defined two- and three-body virial coefficients in which the repulsive and attractive interaction strength and range are inextricably lumped together.

B. Semidilute Regime: Osmotic Pressure and Screening Length. For treating the polymer concentration dependence of the osmotic pressure under good solvent conditions, we choose the intermolecular potential parameters a and d to be intrinsic, that is, independent of temperature, concentration, and N. However, the ratio of segment lengths σ/σ_θ implicit in eq 47 will in general be a function of both concentration and solvent quality. For a given method of choosing the semidilute crossover density ρ_m^*, the onset of the concentrated regime at ρ_m^{**}, and the dilute solution scaling exponent ν_F, we construct the following piecewise continuous, minimalist model for the polymer concentration dependence of the ratio of effective segment lengths:

$$\frac{\sigma}{\sigma_\theta} = 1, \quad \rho_m > \rho_m^{**}$$

$$\frac{\sigma}{\sigma_\theta} = \left[\frac{\rho_m}{\rho_m^{**}}\right]^{(1-2\nu_F)/(6\nu_F-2)}, \quad \rho_m^{**} > \rho_m > \rho_m^*$$

$$\frac{\sigma}{\sigma_\theta} = \left[\frac{\rho_m^*}{\rho_m^{**}}\right]^{(1-2\nu_F)/(6\nu_F-2)}, \quad \rho_m^* > \rho_m \qquad (60)$$

Equation 60 corresponds to assuming that, in the melt/concentrated regime, the chain dimensions are unperturbed. The concentration dependence of σ adopted in eq 60 corresponds to the blob scaling theory prediction[2] for the semidilute regime and the experiments of Cotton et al.[54] Since we employ a model in which σ is concentration-dependent, the monomer densities are expressed in terms of σ_θ^{-3}. In these units, the maximum possible monomer density, corresponding to the divergence in the athermal pressure in the string model, is given by

$$\rho_{max}\sigma_\theta^3 = \frac{9}{2\pi}\left(\frac{\sigma_\theta}{d}\right) \qquad (61)$$

The density corresponding to the crossover into the semidilute regime is estimated from the usual coil overlap condition introduced in eq 17, where R_g in eq 17 is to be evaluated in the dilute regime. Use of eqs 17 and 60 leads to the following expression for ρ_m^*:

$$\rho_m^*\sigma_\theta^3 \approx \left[\frac{9\sqrt{6}}{2\pi\sqrt{N}}\right]^{(6\nu_F-2)}\left[\frac{1}{\rho_m^{**}\sigma_\theta^3}\right]^{(6\nu_F-3)} \qquad (62)$$

Equations 60 and 62 are consistent with the standard relations $\rho_m^* \sim N^{(1-3\nu_F)}$ and $R_g \sim N^{\nu_F}$ in dilute solution.

We identify the crossover to the concentrated regime, ρ_m^{**}, as the density at which the pressure for the athermal string fluid starts deviating significantly from a z^3 power-law scaling increase based on extrapolation of the semidilute behavior. This criterion, applied to the results shown in Figures 1 and 2, leads to the estimate that

$$\rho_m^{**} \approx 0.18\rho_{max} \qquad (63)$$

In our comparison in section III to simulations for the athermal pressure, we identified the maximum permissible monomer density, ρ_{max}, with a packing fraction $\eta = 1/\sqrt{2}$. If we now associate the dense melt with the liquid-like packing fraction[17] of $\eta = {}^1/_2$, we are led to the following estimate for the melt monomer density in terms of ρ_{max}:

$$\rho_{melt} = \frac{\rho_{max}}{\sqrt{2}} \qquad (64)$$

From eqs 63 and 64, the crossover to the concentrated regime is predicted to occur at a concentration corresponding to ≈25% polymer by volume.

Given the model for the concentration dependence of σ presented in eq 60, the general expression for the compressibility route pressure in eq 42, and the PRISM result in eq 10 for ξ_ρ in the thread model, the density dependence of the pressure in the athermal thread limit is predicted to be

$$\sigma_\theta^3\beta P = \frac{\rho_m\sigma_\theta^3}{12\xi_c^2} + \frac{\pi(\rho_m\sigma_\theta^3)^2}{36\xi_c}\left(\frac{\sigma_0}{\sigma_\theta}\right)^2 + \frac{\pi^2(\rho_m\sigma_\theta^3)^3}{324}\left(\frac{\sigma_0}{\sigma_\theta}\right)^3, \quad \rho_m < \rho^*_m$$

$$\sigma_\theta^3\beta P = \sigma_\theta^3\beta P(\rho^*_m) + \frac{1}{12\xi_c^2}[\rho_m\sigma_\theta^3 - \rho^*_m\sigma_\theta^3] + \frac{\pi(6\nu_F-2)}{18\xi_c(6\nu_F-1)}(\rho^{**}_m\sigma_\theta^3)^{(6\nu_F-3)/(6\nu_F-2)} \times [(\rho_m\sigma_\theta^3)^{(6\nu_F-1)/(6\nu_F-2)} - (\rho^*_m\sigma_\theta^3)^{(6\nu_F-1)/(6\nu_F-2)}] + \frac{\pi^2(3\nu_F-1)}{324\nu_F}(\rho^{**}_m\sigma_\theta^3)^{(6\nu_F-3)/(3\nu_F-1)}[(\rho_m\sigma_\theta^3)^{3\nu_F/(3\nu_F-1)} - (\rho^*_m\sigma_\theta^3)^{3\nu_F/(3\nu_F-1)}], \quad \rho^*_m < \rho_m < \rho^{**}_m$$

$$\sigma_\theta^3\beta P = \sigma_\theta^3\beta P(\rho^{**}_m) + \frac{1}{12\xi_c^2}[\rho_m\sigma_\theta^3 - \rho^{**}_m\sigma_\theta^3] + \frac{\pi}{36\xi_c}[(\rho_m\sigma_\theta^3)^2 - (\rho^{**}_m\sigma_\theta^3)^2] + \frac{\pi^2}{324}[(\rho_m\sigma_\theta^3)^3 - (\rho^{**}_m\sigma_\theta^3)^3], \quad \rho_m > \rho^{**}_m \qquad (65)$$

In the above equation, ξ_c is in units of σ, i.e., $\xi_c \equiv (N/12)^{1/2}$. In the concentrated or melt-like regime ($\rho_m > \rho^{**}_m$), the pressure grows like $P \sim \rho_m^3$ (the semidilute Θ solvent scaling law), and this is the domain in which the distinction between string and thread models is most apparent. For the string model, the integration in eq 47 cannot be performed analytically, as ξ_ρ must be determined by numerical solution of a transcendental equation (eq 23).

Figure 4 shows model calculations for the reduced osmotic pressure or "compressibility factor", $P/k_BT\rho_m$, as a function of ρ_m/ρ_{melt} for various chain lengths N, with

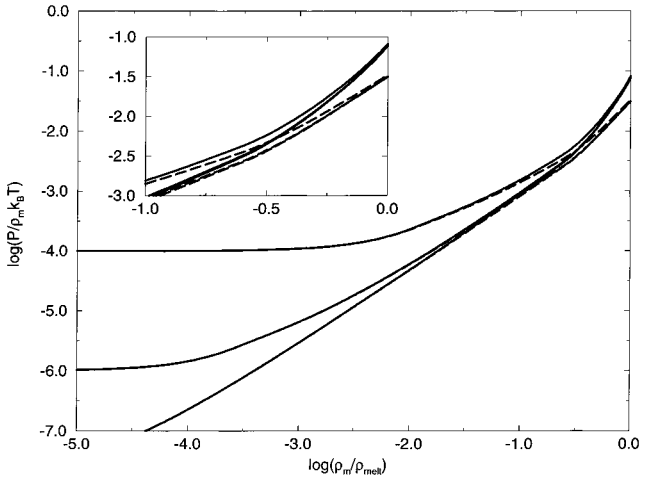

Figure 4. Log−log plot of the reduced osmotic pressure as a function of reduced polymer density; the solid and broken lines correspond to the athermal string and thread models, respectively. For each set of curves, from bottom to top, $N = 10^8$, 10^6, and 10^4; the parameters used are $d = \sigma_\theta$ and $\nu_F = 0.6$. The inset shows a magnified portion of the main figure for high polymer densities, including the crossover from the semidilute to concentrated regimes.

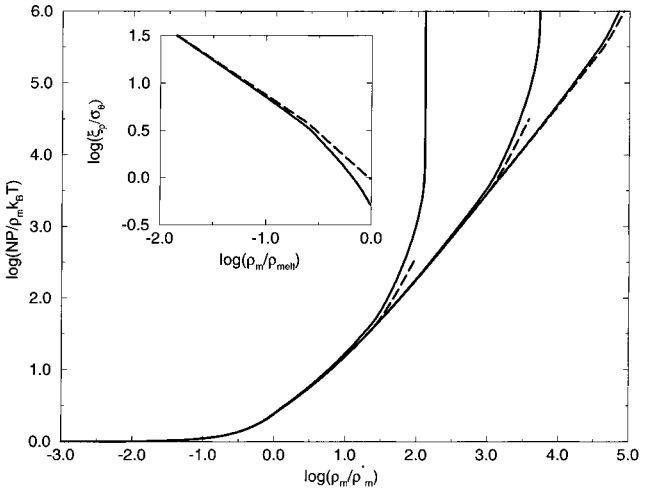

Figure 5. Reduced osmotic pressure on a per molecule basis as a function of scaled polymer density ρ_m/ρ_m^*; the solid and broken lines correspond to the athermal string and thread models, respectively. From left to right, the curves correspond to $N = 10^4$, 10^6, and 10^8; parameters used are the same as in Figure 4. The inset shows the athermal density screening length $\log(\xi_\rho/\sigma_\theta)$ as a function of $\log(\rho_m/\rho_{melt})$ for $N = 10^8$ and $d = \sigma_\theta$; the solid and broken lines represent the string and thread model predictions, respectively.

$d = \sigma_\theta$ and $\nu_F = 0.6$. In the dilute regime, P obeys the trivial ideal solution/Van't Hoff law. In the semidilute regime, the slope of P increases monotonically with ρ_m, and for the longer chains the $P \sim \rho_m^{9/4}$ law is approached inside the semidilute regime. In the concentrated regime ($\rho_m > \rho^{**}_m$), the curves for various N merge and P becomes effectively independent of chain length. Note that the thread and string model predictions for a given value of N are virtually identical for $\rho_m < \rho^{**}_m$.

The above features are also seen in Figure 5, in which, for the same model, we examine $NP/k_BT\rho_m$ as a function of ρ_m/ρ_m^*. In the main part of Figure 5, the curves for various N merge in the dilute and semidilute regimes but become distinct as $\rho_m > \rho_m^{**}$, since the ratio ρ_m^{**}/ρ_m^* is an N-dependent quantity. The inset in Figure 5 shows a double-logarithmic plot of the density screening length ξ_ρ, in units of σ_θ, as a function of ρ_m/ρ_{melt}, for the thread and string models. In the semidilute regime ξ_ρ is well-described by $\xi_\rho \sim \rho_m^{-0.75}$; for $\rho_m > \rho_m^{**}$, ξ_ρ diminishes much more rapidly in the string model, corresponding to the more rapid increase in the pressure.

Experimental data for different good solvents and chain lengths for PS lead to the following empirical equation[9] for the concentration dependence of ξ_ρ in the semidilute regime:

$$\xi_\rho = (0.27 \pm 0.1)C^{-0.72\pm0.01} \tag{66}$$

where the polymer concentration C is in grams per milliliter and ξ_ρ is in nanometers. The above relation applies for solutions up to about 30% polymer by concentration. Extrapolation of eq 66 to the melt density (1.06 gm cm^{-3}) leads to the estimate that $\xi_\rho \approx 2.6 \pm 1$ Å in PS neat melts. For a solution at 25% polymer concentration, which corresponds approximately to the estimate for ρ_m^{**} in our present model, eq 66 suggests that, for PS, $\xi_\rho \approx 7.1 \pm 2.7$ Å. For the athermal string model, solution of eq 25 shows that, at "melt-like" densities ($\psi/\psi_{max} = 1/\sqrt{2}$), the screening length is $\xi_\rho \approx d/2$; at $\rho_m = \rho_m^{**}$, that is, when $\psi^{**}/\psi_{max} = 0.18$, we find from eq 25 that $\xi_\rho \approx 3d$. For PS in toluene, if we choose a statistical segment length $\sigma_\theta = 7.058$ Å and an aspect ratio $\Gamma_\theta = 1$ as in section V.A, we find that the string model predicts $\xi_\rho \approx 20$ Å at ρ_m^{**} and $\xi_\rho \approx 3.5$ Å at the "melt-like" density. The near agreement with the value of ξ_ρ obtained by extrapolation of the experimental data to melt-like densities is probably fortuitous, as the semidilute scaling law should not be expected to be applicable up to melt-like density. This is reflected in the fact that ξ_ρ calculated this way from the string model is greater by a factor of 2 or so than that measured experimentally at 25% polymer concentration (ρ_m^{**}).

Figure 6 compares the concentration dependence of $NP/\rho_m k_B T$ predicted by the string PRISM theory to the experimental measurements[29] of Noda et al. on the system poly(α-methylstyrene) plus toluene. For this comparison, we use the experimentally determined value of the Flory exponent for this system,[29] $\nu_F = 0.585$, in eqs 47 and 60, and $d = \sigma_\theta$. As in our calculation of the second virial coefficient B_2, each α-methylstyrene monomer is taken to correspond to a single string model site. A value of $N = 65\,400$ is employed, roughly equal to the degree of polymerization of the largest chains investigated by Noda et al. Also shown (broken line) is the result obtained from a renormalization-group calculation by Ohta and Oono;[8] in their calculation, as in ours, there exists a degree of ambiguity in the precise assignment of ρ_m^*, which is treated by those authors as a fitting parameter. We find that our calculation, while not in as good quantitative agreement with the experimental data as the far more complicated RG calculation, does capture the upturn in the slope at $\rho_m \approx \rho_m^*$, and the ρ_m dependence of P is qualitatively correct. However, the dilute−semidilute crossover predicted by the string PRISM theory is more rounded and milder; hence, the absolute magnitude of P is somewhat lower than that observed. The circles include experimental measurements for a range of chain lengths;[29] the collapse onto a single curve for $\rho_m < \rho_m^{**}$ for various N is correctly described at the level of thread and string models, as seen in Figures 4 and 5.

C. Concentrated Solutions and Melts. Prior numerical PRISM studies of the equation-of-state of chemically realistic models of specific polymer melts have been published.[55,56] Here we discuss results obtained using the simplified analytic string model for equation-of-state properties in the melt-like regime. In section III it was shown that choosing $\Gamma = 10.3$ for the aspect ratio ($\Gamma = \sigma/d$) led to nearly quantitative agreement with simulations on athermal chains[10] for the density dependence of the repulsive pressure. Therefore, the same model is used in this section to calculate both the attractive and repulsive contributions to the pressure from eq 47. In the compressibility route to the pressure, the inverse structure factor must be integrated over the entire range of densities from zero to the desired density. The adoption of specific models for the concentration dependence of the segment length for use in eq 47 will thus lead to different predictions for the pressure, which differ by a numerical constant in the regime $\rho_m > \rho_m^{**}$; the density dependence of the calculated pressure in this concentrated regime is unaffected, as by hypothesis σ becomes independent of concentration for $\rho_m > \rho_m^{**}$. The pressure as a function of density in the melt regime must, of course, be independent of factors such as solvent quality and chain conformation at lower concentration in an *exact* statistical mechanical theory.

Since in the present section we are concerned only with dense melts, for simplicity we assume the chains to be unperturbed, that is, that σ is independent of ρ_m for all values of ρ_m in performing the integrals in eq 47, which then gives in the long chain limit

$$\sigma^3\beta P_{tot}(\rho_m) = P_{rep}(\rho_m) - \frac{P_{att}(\rho_m)}{T^*} \tag{67}$$

$$P_{rep}(\rho_m) = \frac{\sigma^3}{12}\int_0^{\rho_m} d\rho_1 \left(\frac{\sigma}{\xi_\rho(\rho_1)}\right)^2 \equiv \Gamma^3 f_1(\psi) \tag{68}$$

$$P_{att}(\rho_m) = 2\left(\frac{\nu}{\Gamma}\right)^2 e^{-1/\nu}\sigma^3\int_0^{\rho_m} d\rho_1 \left[2\pi\left(\frac{\nu}{\Gamma}\right)\rho_1\sigma^3\left(1+\frac{1}{\nu}\right) - 6 + \frac{6e^{-d/\xi_\rho(\rho_1)}}{\left(1+\frac{\nu d}{\xi_\rho(\rho_1)}\right)}\right]$$

$$\equiv \frac{2\nu^2 e^{-1/\nu}}{\Gamma} f_2(\psi,\nu) \tag{69}$$

where the reduced density variable ψ was defined in eq 26. The density dependence of the attractive pressure becomes progressively weaker with increasing ρ_m and is nowhere stronger than $P_{att} \sim \rho_m^3$; as ρ_m approaches ρ_{max}, this dependence approaches $P_{att} \sim \rho_m^2$, as in van der Waals theory. We first discuss some qualitative features of eq 67, all of which appear physically reasonable, prior to a more detailed comparison with experimental data for polyethylene (PE) melts.

There are four independent model parameters in eq 67: the reduced temperature T^*, the hard core site diameter d, the range a of the attractive interaction, and the segment length σ. At a fixed value for the dimensionless overall compressibility factor $\sigma^3\beta P_{tot}$ and constant values of all the other model parameters, an increase in the temperature T^* results in a reduction in P_{att} at a given density; thus, to maintain the balance between P_{rep} and P_{att}, the density ρ_m drops as the temperature is raised and the isothermal compressibility κ_T increases. Also, as the density decreases, one moves to a region where P_{rep} is a weaker function of ρ_m than at the lower temperature; thus, the thermal expansion coefficient becomes larger as the temperature is raised at constant pressure. Reducing the interaction range a at constant pressure and T^*, keeping d and σ fixed, reduces the strength of the attractive pressure and has similar effects as increasing the temperature. A reduction in a at constant total pressure, keeping all other parameters unchanged, leads to a reduction in the density and increases in the isothermal compressibility and thermal expansion coefficient.

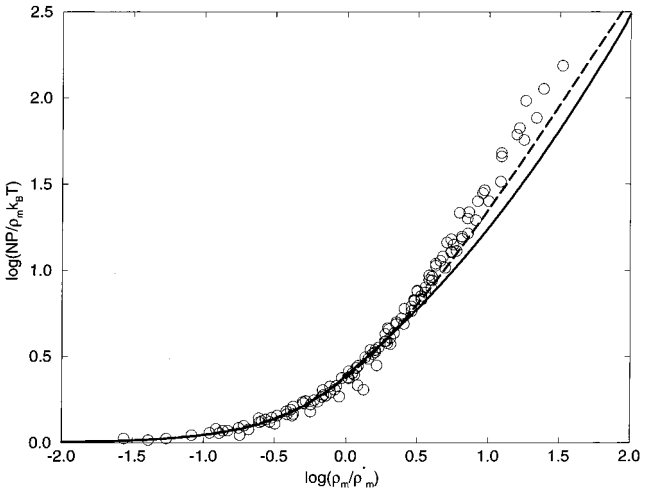

Figure 6. Reduced osmotic pressure on a per molecule basis plotted versus ρ_m/ρ_m^*; the circles show experimental data[29] for poly(α-methylstyrene) in toluene at various chain lengths N. The solid line shows the prediction of the athermal string model, with $N = 65\,400$, $d = \sigma_\theta$, and $\nu_F = 0.585$. The broken line is the prediction of a renormalization group calculation.

The effects of altering the segment length σ keeping all other parameters fixed (or, equivalently, changing the aspect ratio Γ at fixed a, d, and T^*) are more complex. Equation 67 shows that an increase in Γ at fixed a, d, and T^* leads to a reduction in the contribution from P_{att} at a given density; the density must readjust so as to increase the relative contribution from the attractive pressure to maintain the total pressure constant. This implies that a reduction in ψ, and therefore in ρ_m, is caused by increasing σ if all other parameters are kept fixed. This decrease in ρ_m is accompanied by an increase in the isothermal compressibility κ_T ; however, numerical solution of eq 67 shows that the coefficient of thermal expansion exhibits a complex nonmonotonic dependence on σ. It should be emphasized that the qualitative trends mentioned in this and the foregoing paragraph refer to the long chain limit; numerical solution of the analogues of eq 67 for *finite* N shows that, at fixed total pressure, T^*, a, d, and σ, the density is a monotonically increasing function of N which saturates at $N \approx 100$. This prediction is consistent with experiments on homologous members of the alkane series.[57]

We now compare the predictions of eq 67 to measurements of the temperature and pressure dependence of the density for high-molecular-weight linear polyethylene (HMLPE) due to Olabisi and Simha.[58] We equate σ to the statistical segment length of PE; the tabulated[47] $T = 400$ K value of $C_\infty \approx 7$ for PE leads to $\sigma = 4.074$ Å.

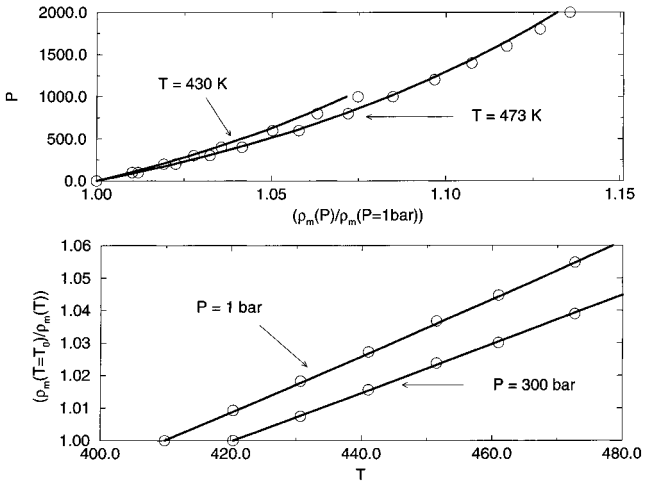

Figure 7. (upper panel) Pressure (in bar) as a function of the normalized monomer density ($\rho_m(P)/\rho_m(P=1$ bar)) at fixed temperature; the circles are experimental data[58] for HMLPE, and the solid lines are the string model predictions, at two temperatures. (lower panel) Temperature dependence of the normalized reciprocal density at two values of fixed pressure; the circles and lines are experimental data[58] for HMLPE and the string model predictions, respectively. The reference temperatures used to normalize the density are $T_0 = 409.85$ K and $T_0 = 420.35$ K at 1 bar and 300 bar, respectively. All theoretical curves use the parameters $\Gamma = 3.15$, $\nu = 2.65$, $|\epsilon|k_B = 60$ K, and $\sigma = 4.074$ Å.

On the basis of this a priori experimental value for σ, there remain three free parameters, a, d, and $|\epsilon|$. We adopt the procedure of fitting the experimentally measured values of the isothermal compressibility and thermal expansion coefficient at 473 K and 1 bar; this process yields $d = 1.293$ Å. The remaining two parameters, a and $|\epsilon|$, may be picked in a number of ways that yield approximately equally good fits to the data; decreasing $|\epsilon|$ has antagonistic effects to increasing a, as noted above, and so long as this *pair* of variables is chosen to fit the isothermal compressibility for $d = 1.293$ Å, it is found that the thermal expansion coefficient is relatively insensitive to the *specific* values of a and $|\epsilon|$. Thus, the calculations shown in Figure 7 should be regarded as a two-parameter fit to the experimental data; given $d = 1.293$ Å and a given (arbitrary) value of a, we then choose $|\epsilon|$ to fit the isothermal compressibility and coefficient of thermal expansion. For concreteness, in the calculations shown in Figure 7, we have picked $a = 3.43$ Å and $|\epsilon|/k_B = 60$ K. The latter value is in the accepted range for a methylene group.[40] Different choices for a and $|\epsilon|$, as mentioned above, correspond to adjusting these parameters to keep the density at approximately the same value at the given pressure.

In the upper part of Figure 7, we show the pressure (in bars) as a function of the density (normalized by its value at atmospheric pressure), for $T = 430$ and 473 *K*. The circles show the data of Olabisi and Simha,[58] and the solid lines represent the prediction of eq 67 with the parameters mentioned above. In the lower part of Figure 7, we show the temperature dependence of the density normalized by its value at the lowest temperature point, at constant pressure, for $P = 1$ and 300 atm; the symbols have the same meanings as in the upper panel of Figure 7. We observe an increase of the compressibility with temperature and its gradual decrease with increasing pressure and density signaled by the upward concavity of the calculated and experimental curves. The theory correctly captures the decrease in the thermal expansion coefficient at elevated pressures, owing to the shift toward higher densities.

In Figure 7, we have presented the results in terms of reduced or normalized densities to highlight the temperature and pressure dependence of this quantity. Conversion of the values obtained for ρ_m using eq 67 into units of gram per cubic centimeter for PE based on the idea that single-string monomers represent individual methylene units leads to $\rho \approx 1.2$ g cm^{-3} at 430 K, about 50% higher than the experimental value.[58] However, in terms of the packing fraction, if we again associate $\eta = 1/\sqrt{2}$ with the maximum density allowed in our model, the above value for ρ corresponds to a packing fraction of about 0.55, a reasonable value for a dense melt.[17]

In closing this section, we comment on the relationship of the present theory to other equations-of-state (EOS) developed for treating one-component polymeric fluids at *high* (melt) densities. Widely-used equations-of-state for polymeric fluids include those due to Flory et al.,[59] Sanchez and Lacombe,[32,33] and various versions of cell and hole models.[60,61] Recently, a new EOS has been developed on the basis of empirical arguments and a Pade analysis of the pressure dependence of the bulk modulus.[62] All of these aforementioned theories satisfy (in the long chain limit) a corresponding states principle empirically known to be valid for polymeric fluids;[63] that is, in all these theories, the EOS can be written in a dimensionless form completely specified by values for the material-specific parameters P', T', and V' for rendering the pressure, temperature, and molar volume dimensionless. These substance-specific parameters are typically determined from a process of curve-fitting, rather than from a priori microscopic arguments.

Eqs 67−69 show that the compressibility route EOS for the string model with RMPY/HTA closure does *not* satisfy a corresponding-states principle. The reason for this is the fact that the attractive pressure in eq 69 includes thermal contributions to *all* virial coefficients and *not* only to B_2 as implied by the van der Waals idea. This point is made most clear if we proceed to the Kac limit[64] by taking $a \to \infty$ and $|\epsilon| \to 0$, keeping $|\epsilon|a^3 =$ constant; in this limit, the mean field treatment of the attractive interactions is expected to become rigorously accurate.[64] Use of the Kac limit, that is, of infinitely weak yet long-ranged attractive interactions, within the RMPY/HTA closure leads to an attractive pressure that is purely quadratic in the density and given by

$$P_{att}^{Kac} = 2\pi\left(\frac{\nu}{\Gamma}\right)^3\left(1+\frac{1}{\nu}\right)e^{-1/\nu}\,\Gamma^2\psi^2 \qquad (70)$$

and is of generalized van der Waals form. The repulsive pressure is still given by eq 68. Use of eqs 70 and 67 shows that, for the string model in the Kac limit, the compressibility route EOS satisfies a corresponding states principle with $P' = \Gamma^2\epsilon'/\sigma^3$, $T' = \epsilon'/\Gamma k_B$, $\rho_m' = 9\Gamma/2\pi\sigma^3$, and $\epsilon' = |\epsilon|(\nu/\Gamma)^3(1 + 1/\nu)e^{-1/\nu}$. This van der Waals-type EOS can also be obtained by requiring that $g^{(0)}(r) = 1$ for all values of r within the RMPY/HTA closure (eq 37); this replacement corresponds to use of the reference molecular mean spherical approximation (RMMSA).[35,36] Deviations from the corresponding states principle in the present theory are thus linked to departures from completely random mixing ($g^{(0)}(r) = 1$ for all r) at the level of the RMPY/HTA closure approximation (eq 37).

VI. Concluding Remarks

We have presented an analytic, liquid-state integral equation theory of polymer solutions, thermodynamic predictions of which have been worked out over the entire range of macromolecule concentration. Comparison with experiments shows that the present theory provides a satisfactory description of solution thermodynamics in the dilute and semidilute regimes under good solvent conditions. Comparison with simulations shows that, under athermal conditions, the theory is capable of describing the purely repulsive pressure at higher densities as well; however, the choice of parameters needed to achieve good agreement in this regime is difficult to motivate on an a priori microscopic basis. A similar situation is found for the thermal calculations at melt densities discussed in section V.C. It is likely that these quantitative discrepancies at high densities are caused in part by the neglect of chain stiffness and the approximate treatment of the hard core exclusion constraint, which are most suspect at melt-like packing fractions.

Treatment of the Θ point case is a delicate problem, as it requires accurate estimates for *both* the attractive and repulsive contributions to B_2. As shown in McMillan−Mayer theory,[65] B_2 contains information about the thermal pair correlation function $g(r)$ from all length scales at infinite dilution of the polymer, and thus the Θ condition would likely depend strongly on local packing considerations. Even for polymers at infinite dilution, the overall packing fraction of the solution as a whole remains liquid-like. Thus, local chain stiffness and the solvent molecule geometry and size may be important. These considerations may explain why the experimentally observed behavior of $T\!\!\!\Theta(N)$ is significantly dependent on the particular choice of Θ solvent.[49,51] The relevance of three-body interactions under near Θ conditions is another complication which is very difficult to incorporate within an integral equation approach.

In future work, we plan to extend the present framework to treat phase separation in polymer solutions and the liquid−vapor critical properties of one-component polymer fluids.[16] Incorporation of effects due to local chain stiffness and the hard core constraint will be investigated via numerical PRISM studies. We also plan to include the effects of solvent quality and polymer concentration on the single-chain structure in a self-consistent manner,[18−22] which may be particularly important in the context of demixing phase transitions in polymer solutions.

Acknowledgment. This work was supported by the Division of Materials Science, Office of Basic Energy Sciences, U.S. Department of Energy, in cooperation with Oak Ridge National Laboratory, and the UIUC Materials Research Laboratory Grant DEFG02-96-ER45439.

Appendix: Free Energy Charging Route to the Athermal Pressure

Our starting point is the well-known equation for the excess pressure for a hard core fluid, obtained by differentiation of the corresponding excess free energy:[13,17]

$$\beta P_{ex} = 2\pi\rho^2{}_m d^3\left[\int_0^1 d\lambda\, \lambda^2 g^{(\lambda)}(\lambda d) + \rho_m \int_0^1 d\lambda\, \lambda^2 \frac{\partial g^{(\lambda)}(\lambda d)}{\partial \rho_m}\right] \quad (A.1)$$

The integration corresponds to charging the hard-core diameter from zero to a finite value, and $g^{(\lambda)}(\lambda d)$ represents the contact value of $g(r)$ given a hard core diameter equal to λd, where d represents the value of the hard core diameter in the final, fully charged state of interest. For the athermal string model, one has from eq 8

$$g^{(\lambda)}(\lambda d) = 1 + \frac{3}{\pi\psi(\lambda)}[e^{-1/\Gamma\xi_\rho(\lambda)} - 1] \quad (A.2)$$

where $\Gamma\xi_\rho(\lambda)$ is given in the $N \to \infty$ limit by the solution to

$$x^2[1 - e^{-1/x}] - xe^{-1/x} = \frac{1}{2}\left[1 - \frac{2\pi\lambda\psi}{9}\right]$$

$$x = \Gamma\xi_\rho(\lambda) \quad (A.3)$$

We see from eqs A.2 and A.3 that the contact value for $g(r)$ in the string model is a function only of the variable $\lambda\psi$, which allows one to simplify eq A.1 using partial integration to obtain

$$\frac{\beta P_{ex}}{\rho_m} = 2\pi\rho_m d^3[g(d) - 2\int_0^1 d\lambda\, \lambda^2 g^{(\lambda)}(\lambda d)] \quad (A.4)$$

Within the athermal string model the contact value for $g(r)$ is always well-behaved. Thus, the pressure calculated from eq A.4 is also finite for all values of the reduced density ψ. Direct comparison with the simulation results of Gao and Weiner[10] (see Figure 1) shows that the pressure from eq A.4 increases too slowly with the density; in fact, at the highest densities, $P(\rho_m)$ calculated from eq A.4 increases no faster than $\rho_m{}^5$. At meltlike densities, corresponding to $\psi \approx \psi_{max}/\sqrt{2}$, the charging route pressure grows approximately as $P \sim \rho_m{}^{3.5}$. This is to be contrasted with the compressibility route calculation, for which $P \sim \rho_m{}^{4.5}$ at comparable densities. We note also that the functional dependence of the pressure on model variables is different than that obtained from the compressibility route:

$$d^3\beta P = 2\pi\left(\frac{\psi}{\Gamma^2}\right)^2 F(\psi) \quad (A.5)$$

where $F(\psi)$ is a function of the reduced density ψ alone. At low densities, the charging route pressure computed from eq A.4 is given by

$$\frac{\beta P}{\rho_m} \approx \frac{\pi^2\psi^2}{24\Gamma^2} \quad (A.6)$$

which does not become independent of the aspect ratio Γ even in the limit $\rho_m \to 0$. In both routes, the pressure behaves as $P \sim \rho_m{}^3$ at low (semidilute) densities, but the prefactors disagree for all values of Γ except $\Gamma = (13.5)^{1/4}$.

References and Notes

(1) Doi, M.; Edwards, S. F. *The Theory of Polymer Dynamics*; Clarendon: Oxford, 1986.

(2) de Gennes, P. G. *Scaling Concepts in Polymer Physics*; Cornell University Press: Ithaca, 1979.
(3) Yamakawa, H. *Modern Theory of Polymer Solutions*; Harper and Row: New York, 1971.
(4) des Cloizeaux, J.; Jannink, G. *Polymers in Solution: Their modelling and structure*; Clarendon: New York, 1990.
(5) Fujita, H. *Macromolecules* **1988**, *21*, 179.
(6) Muthukumar, M.; Edwards, S. F. *J. Chem. Phys.* **1982**, *76*, 2720.
(7) Muthukumar, M. *J. Chem. Phys.* **1986**, *85*, 4722.
(8) Ohta, T.; Oono, Y. *Phys. Lett.* **1982**, *89*, 460.
(9) Brown, W.; Nicolai, T. *Colloid. Polym. Sci.* **1990**, *268*, 977.
(10) Gao, J.; Weiner, J.H. *J. Chem. Phys.* **1989**, *91*, 3168.
(11) Dickman, R.; Hall, C. K. *J. Chem. Phys.* **1986**, *85*, 4108.
(12) Honnell, K. G.; Hall, C. K. *J. Chem. Phys.* **1989**, *90*, 1841.
(13) Chandler, D. In *Studies in Statistical Mechanics VIII*; Montroll, E., Lebowitz, J., Eds.; North-Holland: Amsterdam, 1982; p 274. Chandler, D.; Andersen, H. C. *J. Chem. Phys.* **1972**, *57*, 1930.
(14) Schweizer, K. S.; Curro, J. G. *Adv. Polym. Sci.* **1994**, *116*, 319; *Adv. Chem. Phys.* **1997**, Vol. XCVIII, Chapter 1, pp 1−142.
(15) Chatterjee, A. P.; Schweizer, K. S. In preparation.
(16) Chatterjee, A. P.; Schweizer, K. S. *J. Chem. Phys.* **1998**, in press.
(17) Hansen, J. P.; McDonald, I. R. *Theory of Simple Liquids*, 2nd ed.; Academic: London, 1986.
(18) Grayce, C. J.; Schweizer, K. S. *J. Chem. Phys.* **1994**, *100*, 6846.
(19) Grayce, C. J.; Yethiraj, A.; Schweizer, K. S. *J. Chem. Phys.* **1994**, *100*, 6857.
(20) Melenkevitz, J.; Curro, J. G.; Schweizer, K. S. *J. Chem. Phys.* **1993**, *99*, 5571.
(21) Grayce, C. J.; de Pablo, J. J. *J. Chem. Phys.* **1994**, *101*, 6013.
(22) Yethiraj, A. *Phys. Rev. Lett.* **1997**, *78*, 3789.
(23) Wheeler, J. C.; Chandler, D. *J. Chem. Phys.* **1971**, *55*, 1645.
(24) Kniewske, R.; Kulicke, W. M. *Makromol. Chem.* **1983**, *184*, 2173.
(25) Appelt, B.; Meyerhoff, G. *Macromolecules* **1980**, *13*, 657.
(26) Huber, K.; Bantle, S.; Lutz, P.; Burchard, W. *Macromolecules* **1985**, *18*, 1461.
(27) Bruns, W. *Macromolecules* **1996**, *29*, 2641; **1997**, *30*, 4429.
(28) Douglas, J. F.; Freed, K. F. *Macromolecules* **1985**, *18*, 201.
(29) Noda, I.; Kato, N.; Kitano, T.; Nagasawa, M. *Macromolecules* **1981**, *14*, 668.
(30) Schweizer, K. S.; Curro, J. G. *Chem. Phys.* **1990**, *149*, 105.
(31) Schweizer, K. S.; Szamel, G. *J. Chem. Phys.* **1995**, *103*, 1934.
(32) Sanchez, I. C.; Lacombe, R. *Macromolecules* **1978**, *11*, 1145.
(33) Sanchez, I. C.; Lacombe, R. *J. Phys. Chem.* **1976**, *80*, 2352.
(34) Tonks, L. *Phys. Rev.* **1936**, *50*, 955.
(35) Schweizer, K. S.; Yethiraj, A. *J. Chem. Phys.* **1993**, *98*, 9053.
(36) Yethiraj, A.; Schweizer, K. S. *J. Chem. Phys.* **1993**, *98*, 9080.
(37) Singh, C.; Schweizer, K. S.; Yethiraj, A. *J. Chem. Phys.* **1995**, *102*, 2187.
(38) David, E. F.; Schweizer, K. S. *J. Chem. Phys.* **1994**, *100*, 7767; *Macromolecules* **1997**, *30*, 5118.
(39) Guenza, M.; Schweizer, K. S. *J. Chem. Phys.* **1997**, *106*, 7391.
(40) Schweizer, K. S.; David, E. F.; Singh, C.; Curro, J. G.; Rajasekaran, J. J. *Macromolecules* **1995**, *28*, 1528.
(41) Joanny, J. F.; Leibler, L.; Ball, R. *J. Chem. Phys.* **1984**, *81*, 4640. Broseta, D.; Leibler, L.; Joanny, J. F. *Macromolecules* **1987**, *20*, 1935.
(42) Guenza, M.; Schweizer, K. S. *Macromolecules* **1997**, *30*, 4205.
(43) Berry, G. C. *J. Chem. Phys.* **1966**, *44*, 4550.
(44) Einaga, Y.; Abe, F.; Yamakawa, H. *Macromolecules* **1993**, *26*, 6243.
(45) Nakata, M. *Makromol. Chem.* **1971**, *149*, 99.
(46) Bantle, S.; Schmidt, M.; Burchard, W. *Macromolecules* **1982**, *15*, 1604.
(47) Flory, P. J. *Statistical Mechanics of Chain Molecules*; Oxford: New York, 1969.
(48) Kirste, V. R. G.; Wild, G. *Makromol. Chem.* **1969**, *121*, 174.
(49) Huber, K.; Stockmayer, W. H. *Macromolecules* **1987**, *20*, 1400.
(50) Nakamura, Y.; Norisuye, T.; Teramoto, A. *J. Polym. Sci., Part B: Polym. Phys. Ed.* **1991**, *29*, 153.
(51) Nakamura, Y.; Inoue, N.; Norisuye, T.; Teramoto, A. *Macromolecules* **1997**, *30*, 631.
(52) Yamakawa, H. *Macromolecules* **1992**, *25*, 1912.
(53) Nakamura, Y.; Norisuye, T.; Teramoto, A. *Macromolecules* **1991**, *24*, 4904.
(54) Daoud, M.; Cotton, J. P.; Farnoux, B.; Jannink, G.; Sarma, G.; Benoit, H.; Duplessix, R.; Picot, G.; de Gennes, P. G. *Macromolecules* **1975**, *8*, 804.
(55) Curro, J. G.; Yethiraj, A.; Schweizer, K. S.; McCoy, J. D.; Honnell, K. G. *Macromolecules* **1993**, *26*, 2655.
(56) Yethiraj, A.; Curro, J. G.; Schweizer, K. S.; McCoy, J. D. *J. Chem. Phys.* **1993**, *98*, 1635.
(57) *Comprehensive Organic Chemistry*; Barton, D. H. R., Ollis, W. D., Eds.; Pergamon Press: New York, 1979; Vol. 1.
(58) Olabisi, O.; Simha, R. *Macromolecules* **1975**, *8*, 206.
(59) Flory, P. J.; Orwoll, R. A.; Vrij, A. *J. Am. Chem. Soc.* **1964**, *86*, 3507.
(60) Somcynsky, T.; Simha, R. *Macromolecules* **1969**, *2*, 343.
(61) Dee, G. T.; Walsh, D. J. *Macromolecules* **1988**, *21*, 811, 815.
(62) Sanchez, I. C.; Cho, J.; Chen, W. J. *Macromolecules* **1993**, *26*, 4234.
(63) Sanchez, I. C.; Cho, J. *Polymer* **1995**, *36*, 2929 and references therein.
(64) Kac, M.; Uhlenbeck, G. E.; Hemmer, P. C. *J. Math. Phys.* **1963**, *4*, 216.
(65) Hill, T. L. *Statistical Mechanics: Principles and Selected Applications*; McGraw-Hill: New York, 1956.

MA971460O